Electronic Supplementary Information

Impact of Cationic Molecular Length of Ionic Liquid Electrolytes on Cell Performances of 18650 Supercapacitors

Experimental section

Materials and Chemical reagents

1-Ethyl-3-methylimidazolium bis(trifluoromethyl sulfonyl)imide ($C_8H_{11}F_6N_3O_4S_2$) (>97%, Sigma-Aldrich), bromopentane ($CH_3(CH_2)_3Br$) (99%, Sigma-Aldrich), bromobutane ($CH_3(CH_2)_4Br$) (99%, Sigma-Aldrich), bromopropane ($CH_3(CH_2)_2Br$) (99%, Sigma-Aldrich), bromoethane (CH_3CH_2Br) (99%, Sigma-Aldrich), lithium bis(trifluoromethylsulfonyl)imide (LiTFSI) (99%, Sigma-Aldrich), acetonitrile (CH_3CN) (99%, Sigma-Aldrich), 1-methylimidazole ($CH_3C_3H_3N_2$) (99%, Sigma-Aldrich), diethyl ether (DE) (99%, Sigma-Aldrich), silver nitrate ($AgNO_3$) (Sigma-Aldrich), carbon black or CB (super P, 99 %, Alfa Aesar), activated carbon (MTI (TF-B520), carboxymethyl cellulose or CMC (battery grade, Geon), styrene butadiene rubber or SBR (battery grade, Gelon), N-Methyl-2-pyrrolidone (NMP, 99%, Qrec) and polyvinylidene fluoride (PVDF, Sigma-Aldrich) are of analytical grade and without further purification. Deionized (DI) water (15 MΩ.cm) was obtained from Milli-Q system (Millipore).

Synthesis of room-temperature ionic liquids (RTILs)

RTILs composing of imidazolium-based cations with different size of alkyl chain and bis(trifluoromethyl sulfonyl)imide (TFSI) anion were synthesized, via anionic exchange process.[1] Briefly, the 1-alkyl-3-methylimidazolium bromide (CXIMI-Br; X = number of carbon in alkyl

chain) with various alkyl chains including C2IMI-Br, C3IMI-Br, C4IMI-Br, and C5IMI-Br.The dissolution of 1-methylimidazole with 0.14 mol was performed in 10 mL of acetonitrile containing 0.14 mol of bromoalkane. Subsequently, a reflux method was carried out at 80 ˚C for overnight, the colour of solution was then transformed from colourless to yellow. Impurities in the mixture were further removed by utilizing diethyl ether (DE). Lastly, DE was eliminated by the evaporation approach.

The ion-exchange process of Br to TFSI was further carried out for which 0.12 mol of CXIMI-Br was dropped in DI water. Then, lithium bis(trifluoromethyl sulfonyl)imide (LiTFSI) with 0.12 mol was added into the solution and stirred for 4 h. The mixture then occurred the two-layer separation. After that, the solution was washed using DI water till precipitation was disappeared after adding $AgNO_3$. Finally, the products containing the imidazolium cation and TFSI anion were dried by evaporation of moisture. The as-synthesized RTILs with yellow colour were then characterized extensively by nuclear magnetic resonance (NMR) and thermogravimetric analysis (TGA) (see the supplementary information).[1]

Electrode fabrication and electrochemical evaluation in half-cell configuration

For the optimization steps, the electrode and electrolytes were tested in 2032 coin-cell configuration. The electrode for the coin-cell configuration consisted of 8:1:1 of AC: CB: PVDF mass ratio, following our previous report.[2-6] The materials were dispersed in NMP solvent to produce the slurry ink and then coated on carbon fibre paper (CFP) by a spray coating. In the case of a three-electrode system, the CFP was cut to 1 x 1 cm^2 containing ~1 mg of active mass. A three-electrode system was set up in an Ar-filled glove box (Mbraun) with < 1 ppm of O_2 and H_2O. This system consisted of the as-fabricated electrode as a working electrode, the Ag/Ag^+ reference

electrode, and the Pt rod as the counter electrode. The as-synthesized ionic liquid was used as the electrolyte. Cyclic voltammogram (CV) and electrochemical impedance spectroscopy (EIS) were carried out to evaluate the electrochemical performance of the electrodes using Met ohm AUTOLAB potentiostat (PGSTAT302N) operated with the NOVA 1.11 software. The specific capacitance (C_{cv}) was calculated from the CV result following equation S1.[7]

$$C_{cv} = (\int IdV/v)/ (m\Delta V) \quad \text{(S1)}$$

where $\int IdV$ is the area under the discharge curve of the CV profile, v is the scan rate (V/s), ΔV is the discharge potential window (V), and m is the mass of active material on the electrode (g).

Equation S2 was used to calculate the relaxation time constant (τ_0) of the devices. The complex power analysis chart (normalized complex power vs. frequency), which is the resonance frequency plots of |P|/|S| and |Q|/|S|, could be used to calculate f_0 (maximum frequency). The S(ω), P(ω), and Q(ω) were obtained from equations S3 to S7;[8, 9]

$$\tau_0 = 1/(2\pi f_0) \quad \text{(S2)}$$

$$S(\omega) = P(\omega) + jQ(\omega) \quad \text{(S3)}$$

$$P(\omega) = \omega C''(\omega) |\Delta V_{rms}|^2 \quad \text{(S4)}$$

$$Q(\omega) = -\omega C'(\omega) |\Delta V_{rms}|^2 \quad \text{(S5)}$$

$$C'(\omega) = -Z''(\omega)/[\omega |Z(\omega)|^2] \quad \text{(S6)}$$

$$C''(\omega) = Z'(\omega)/[\omega |Z(\omega)|^2] \quad \text{(S7)}$$

where P(ω) and Q(ω) are active power and reactive power, respectively, derived from the real part and the imaginary part. $|V_{rms}|^2 = V_{max}/((\sqrt{2})V_{max})$ corresponds to the maximal amplitude of the applied ac signal, j represents a unit imaginary number and ω is calculated from 2πf (angular frequency). C′(ω) and C″(ω) refer to complex capacitance from real part and the imaginary part. Z′ and Z″ are attributed to real and imaginary parts of the complex impedance Z.

Industrial scale production of 18650 cylindrical supercapacitor prototypes

The large-scale production of the electrode for 18650 cylindrical cells was processed in a dry room production plant with a dew point of -45 °C. The electrode was semi-automatically produced by a roll-to-roll coating technology. To change the solvent system from NMP to DI water, CMC and SBR were used instead of PVDF as a binder for the up-scale process. The mass ratio of AC: CMC: SBR: CB 96.6: 1.3: 1.2: 0.9 was utilized as the optimized ratio for the electrode preparation. First, the materials were added in DI water to prepare the slurry ink. The vacuum mixer was used to prepare the ink with the control viscosity of ~4,000 to 6,000 mPas. The ink mixture was further pasted on Al foil (two sides) at 120 ˚C for the solvent to evaporate by a roll-to-roll coating system. Afterwards, the as-coated electrode was compressed by 10 tons force via an electric calendar machine, and the electrode was then cut to the size of 5.6 x 44 cm^2 through a slitting machine. Lastly, the as-prepared electrode was obtained.

For the fabrication of the symmetric supercapacitors with cylindrical configuration, the as-prepared electrodes were utilized as both negative and positive electrodes with the tri-layer (PP/PE/PP; Polypropylene/Polyethylene/Polypropylene) separator and as-synthesized IL electrolytes. By using an automatic winding machine, the electrodes with

the polymer separator were winded altogether. Next, 6 g of the as-synthesized electrolytes were injected into the cell in an Ar-filled glovebox with the concentration of O_2 and H_2O < 1 ppm and then the cells were transferred under vacuum for 12 h to assure that the electrodes were wet by the IL electrolyte. The automatic crimping machine was further utilized to seal the case. Eight Channel Battery Analyzer (MTI) was used to evaluate the electrochemical performance of 18650 supercapacitor via galvanostatic charge/discharge (GCD) approach.

The gravimetric capacitance (C_{GCD}) from GCD method was calculated according to the equation S8. The gravimetric energy (E) and power (P) densities were determined according to Equations S9 and S10, respectively [7, 10];

$$C_{GCD} = \frac{(I\Delta t)}{(m\Delta V)} \quad \text{(S8)}$$

$$E = \frac{1}{2}C(\Delta V)^2 \quad \text{(S9)}$$

$$P = \frac{E}{\Delta t} \quad \text{(S10)}$$

where I is the applied current (A), Δt is the discharging time (s), ΔV is the potential window of the discharging process excluding the iR drop, and m is the weight (unit in gram) of AC on the electrode or the weight of overall supercapacitor cell including cylindrical case, electrolyte, and electrode.

To evaluate equivalent series resistance (ESR) and equivalent distributed resistance (EDR), GCD technique was used. The as-fabricated cell was charged to a maximum voltage of 3

V and was held for 30 min. After that, the discharge process was processed. ESR and EDR were calculated from equations (S11) and (S12), respectively.

$$ESR = iR_{drop}/I \quad (S11)$$

$$EDR = \Delta V_3/I \quad (S12)$$

An example for evaluating the ESR and EDR is shown in Fig. S9.

Material Characterizations

High-resolution transmission electron microscope or HR-TEM, performed at 120 kV (model, Hitachi) and field-emission scanning electron microscope or FE-SEM operated at 15 kV (JSM-7001F, JEOL) were used to observe the samples' morphology. To characterize the chemical structure of the materials, Raman spectrometer (Bruker Senterra Dispersive Raman microscope at 532 nm of laser wavelength) was used. X-ray diffraction or XRD pattern was taken by Bruker D8 ADVANCE with Cu K_α radiation (40 mA, 40 kV, $\lambda = 1.5418$ Å). To characterize molecular structure of RTILs, ^1H and ^{13}C nuclear magnetic resonance (^1H and ^{13}C NMR) spectra were recorded using Bruker Ascend 600 NMR spectrometer coupling with atmospheric-pressure chemical ionization (APCI) mass spectrometer (Bruker Compact QTOF). Rheological properties of the ionic liquid were tested using a rheometer (Discovery HR 30, TA Instruments). Although the tests were done under ambient condition, the ionic liquids were taken out from an Ar-filled glovebox right before the measurements, and each measurement was done within 90 min after air exposure. About 1.5 mL of the ionic liquids were added to a 40 mm parallel plate

geometry with 1 mm gap height. After allowing the ionic liquids to reach thermal equilibrium at 25 °C, their viscosities were recorded as a function of shear rate from 1000 to 0.1 s^{-1}.

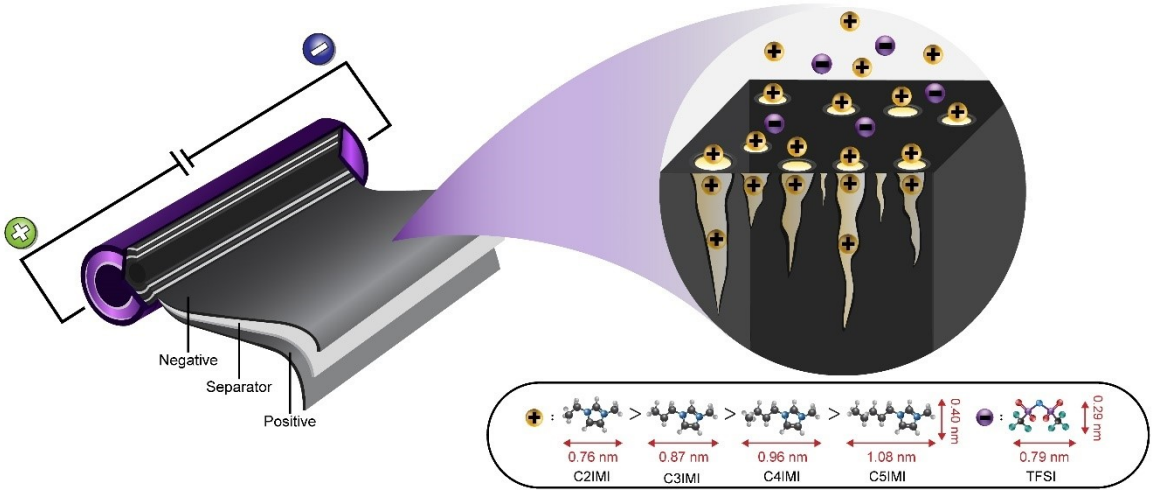

Fig. S1 Schematic showing the cylindrical supercapacitor of microporous activated carbon (AC) materials using ionic liquid electrolytes with different cationic molecules and lengths.

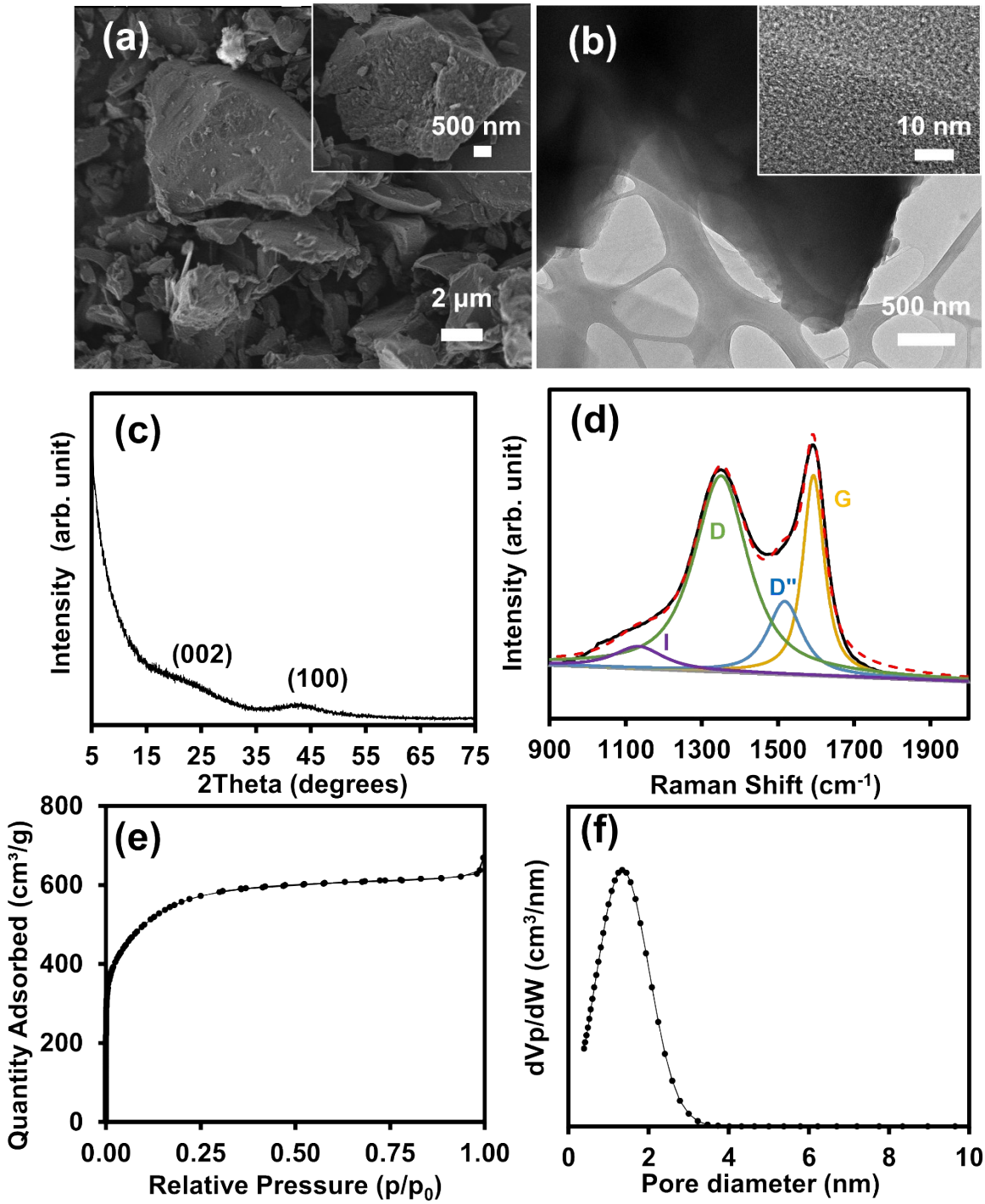

Fig. S2 FE-SEM (a), TEM images (b), XRD pattern (c), Raman spectrum (d), N_2 adsorption-desorption isotherm (e) and pore diameter distribution (f) of AC.

Characterization of the as-synthesized IL

The chemical shifts (δ/ppm) from ^{1}H NMR spectra of imidazolium-based bis(trifluoromethanesulfonyl)imide (IMI-TFSI) have been showed below and in fig. S5A.

C2IMI-TFSI (δ/ppm) = 1.42 ($C\underline{H}_3CH_2N$), 3.86 ($NC\underline{H}_3$), 4.20 ($CH_3C\underline{H}_2N$), 7.65-7.75 ($NC\underline{H}_2C\underline{H}_2N$) and 9.10 ($NC\underline{H}N$),

C3IMI-TFSI (δ/ppm) = 0.84 (t, $C\underline{H}_3CH_2CH_2$), 1.80 (m, $CH_3C\underline{H}_2CH_2$), 3.89 (s, $C\underline{H}_3N$), 4.17 (t, CH_2CH_2N), 7.81-7.89 (dd, $NC\underline{H}C\underline{H}N$) and 9.41 (s, $NC\underline{H}N$)

C4IMI-TFSI (δ/ppm) = 0.88 ($C\underline{H}_3CH_2CH_2$), 1.25 ($CH_3C\underline{H}_2CH_2$), 1.77 ($CH_3CH_2C\underline{H}_2$), 3.89 ($C\underline{H}_3N$), 4.21 ($CH_2C\underline{H}_2N$), 7.80-7.90 ($NC\underline{H}C\underline{H}N$) and 9.41 ($NC\underline{H}N$)

C5IMI-TFSI (δ/ppm) = 0.90 ($C\underline{H}_3CH_2CH_2$), 1.31 ($CH_3C\underline{H}_2CH_2$), 1.37 ($CH_3CH_2C\underline{H}_2$), 1.88 ($C\underline{H}_2CH_2N^+$), 3.94 ($C\underline{H}_3N^+$), 4.16 ($CH_2C\underline{H}_2N^+$), 7.35 ($C\underline{H}C\underline{H}$) and 8.70 ($NC\underline{H}N$)

For ^{13}C NMR spectra of synthetic ILs, the spectra reveal chemical shifts as following and in fig. S5B.

C2IMI-TFSI (δ/ppm) = 15.2 ($\underline{C}H_3CH_2N$), 36.5 ($\underline{C}H_3N$), 44.6 ($CH_3\underline{C}H_2N$), 122.5 ($N\underline{C}HCHN$), 123.5 ($NCH\underline{C}HN$), 120.0 (q, $\underline{C}F_3SO_2N$) and 136.5 ($N\underline{C}HN$).

C3IMI-TFSI (δ/ppm) = 10.8 ($\underline{C}H_3CH_2CH_2N$), 23.3 ($CH_3\underline{C}H_2CH_2N$), 36.2 ($\underline{C}H_3N$), 50.8 ($CH_3CH_2\underline{C}H_2N$), 122.5 ($N\underline{C}HCHN$), 124.0 ($NCH\underline{C}HN$), 120.0 (q, $\underline{C}F_3SO_2N$) and 137.0 ($N\underline{C}HN$)

C4IMI-TFSI (δ/ppm) = 13.6 ($\underline{C}H_3CH_2CH_2CH_2N$), 19.2 ($CH_3\underline{C}H_2CH_2CH_2N$), 31.8 ($CH_3CH_2\underline{C}H_2CH_2N$), 36.2 ($\underline{C}H_3N$), 49.5 ($CH_3CH_2CH_2\underline{C}H_2N$), 122.5 ($N\underline{C}HCHN$), 124.0 ($NCH\underline{C}HN$), 120.0 ($\underline{C}F_3SO_2N$) and 137.0 ($N\underline{C}HN$)

C5IMI-TFSI (δ/ppm) = 13.5 ($C\underline{H}_3CH_2CH_2$), 21.8 ($CH_3C\underline{H}_2CH_2$), 28.1 ($CH_3CH_2C\underline{H}_2$), 29.6 ($CH_2CH_2C\underline{H}_2$), 36.4 ($\underline{C}H_3N$), 50.1 ($CH_3CH_2\underline{C}H_2N$), 122.5 ($N\underline{C}HCHN$), 123.5 ($N\underline{C}HCHN$), 121.0 $(\underline{C}F_3SO_2)_2N$ and 136.0 ($N\underline{C}HN$)

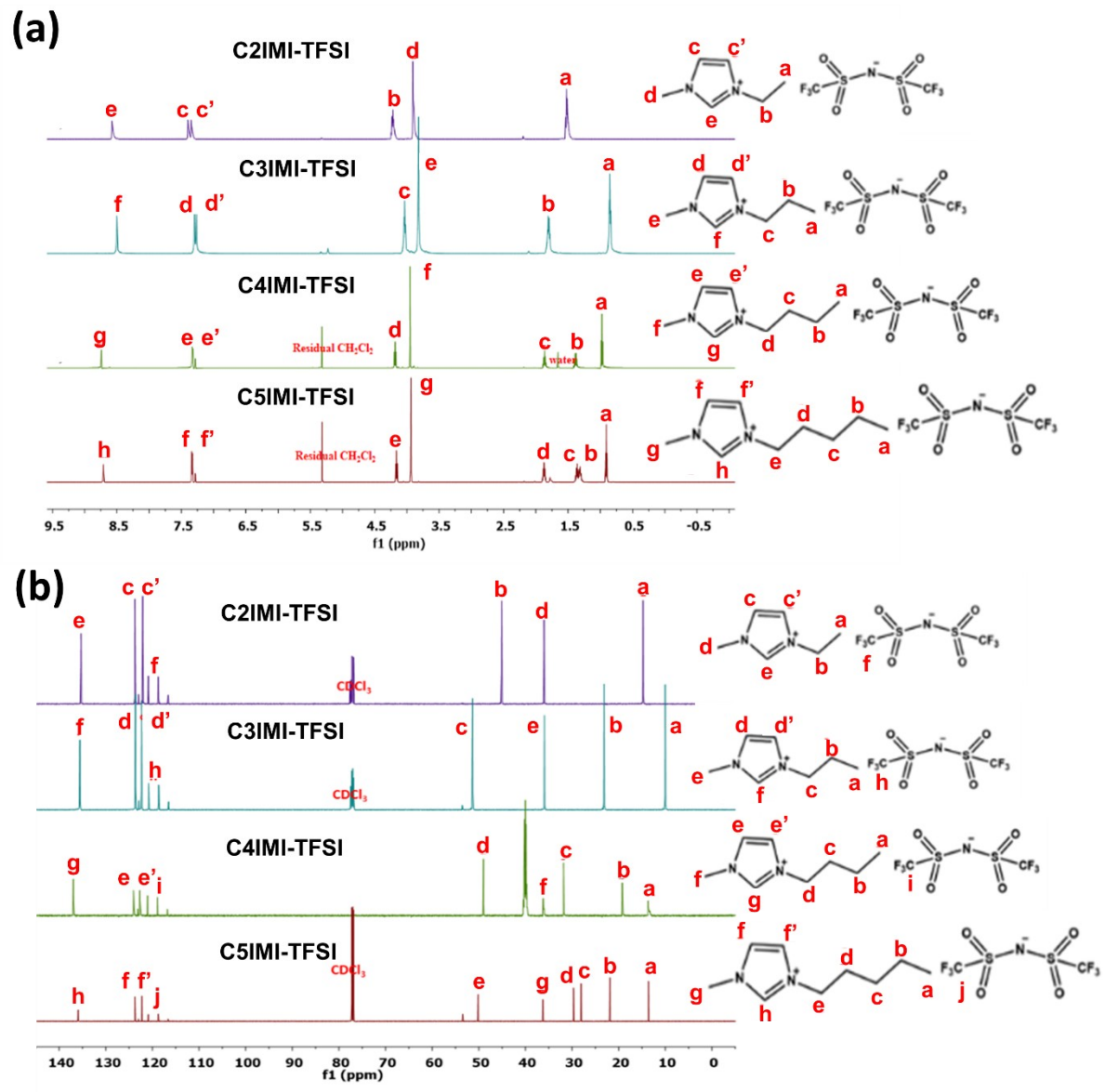

Fig. S3 (a) ^{1}H and (b) ^{13}C NMR of synthesized IL electrolytes.

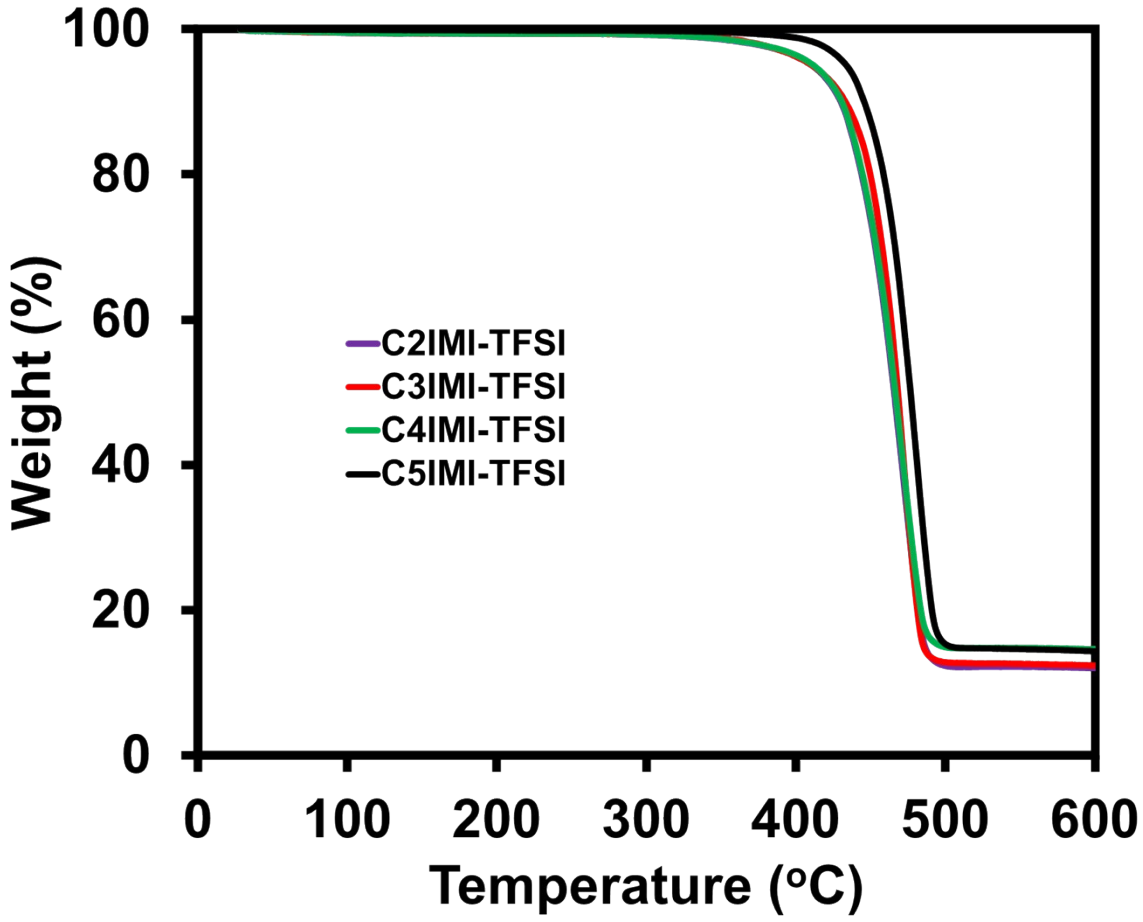

Fig. S4 TGA of various RTILs.

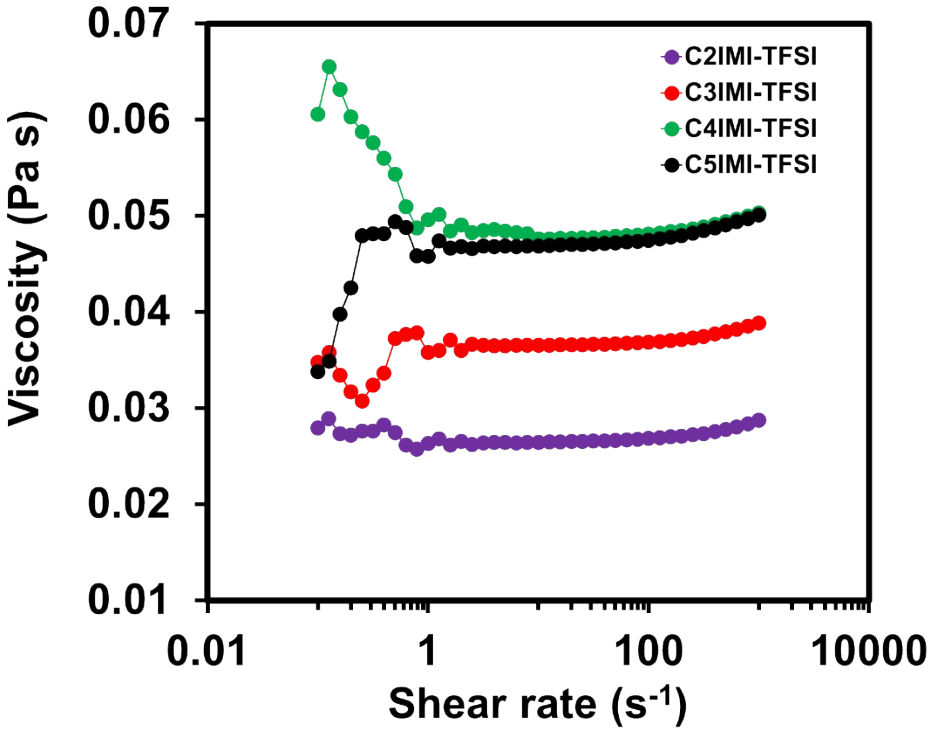

Fig. S5 Viscosity versus shear rate for all ILs at 25 °C.

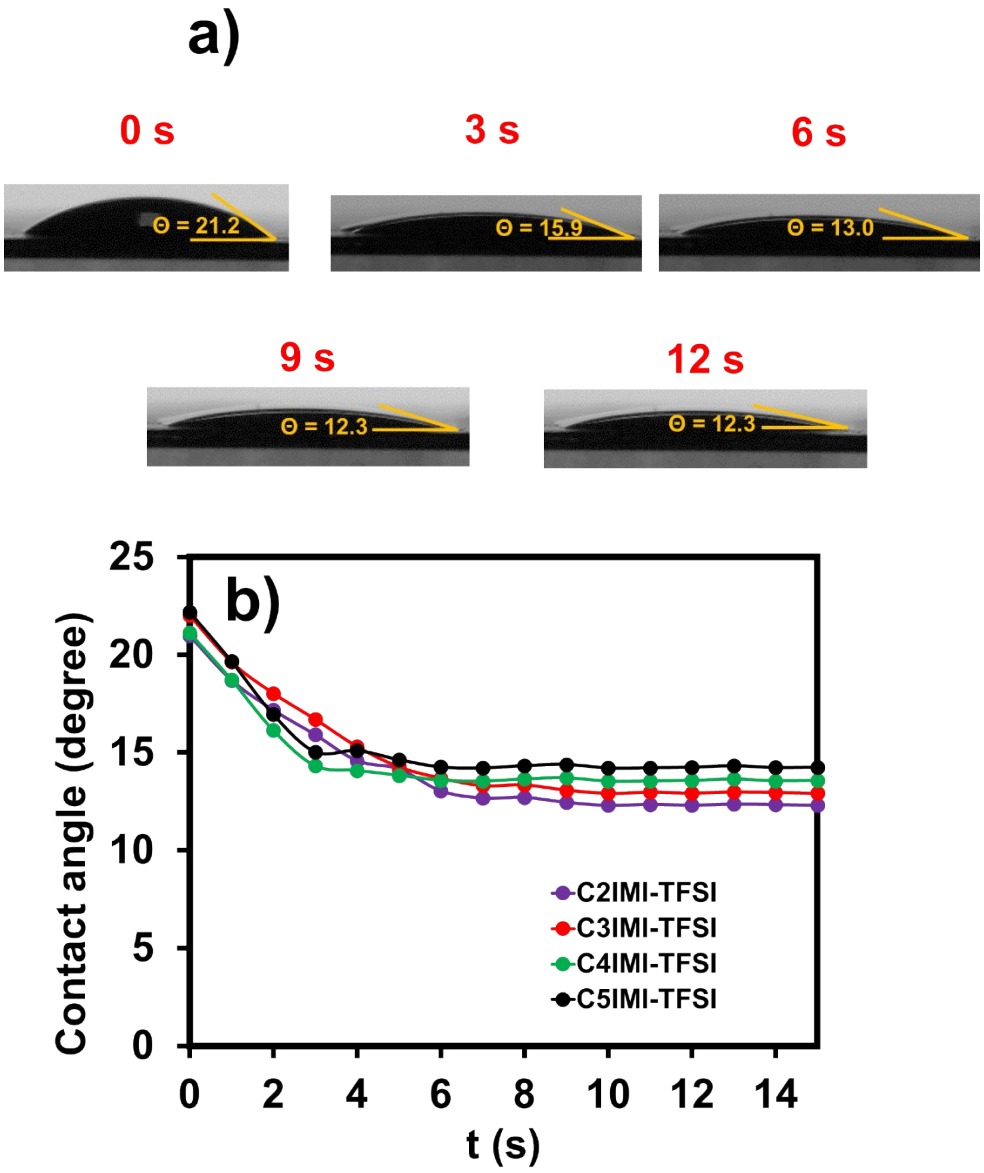

Fig. S6 Optical images showing contact angle of C2IMI-TFSI on AC surface (a) and contact angle of all IL electrolytes depended on the contact time on AC surface (b).

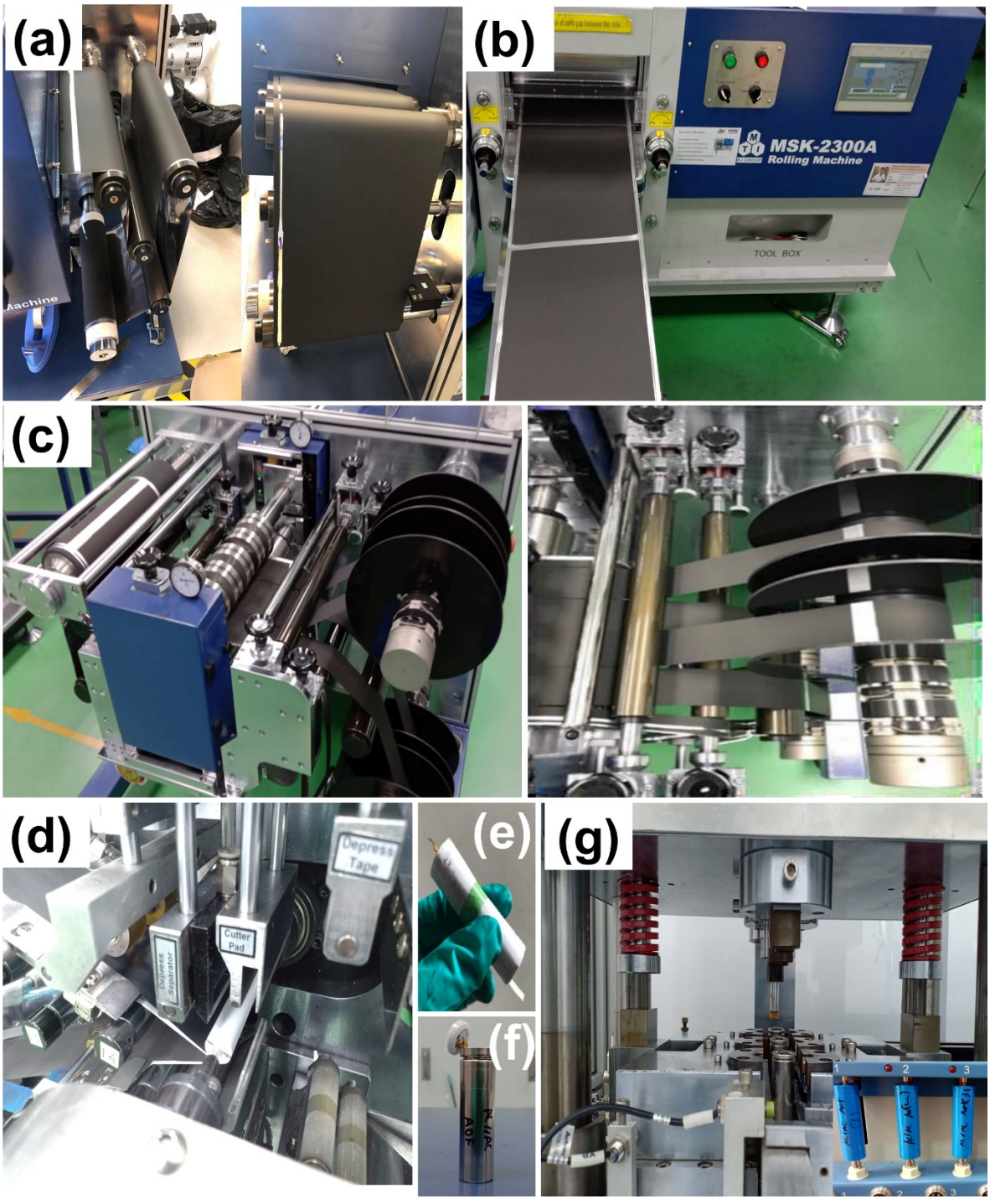

Fig. S7 Fabrication process of 18650 cylindrical supercapacitor. (a) coating process, (b) calendaring of electrode, (c) slitting of electrode, (d) winding method, (e) as-winded electrode, (f) as-welded electrodes with the case, and (g) crimping of cell (inset; as-fabricated cell).

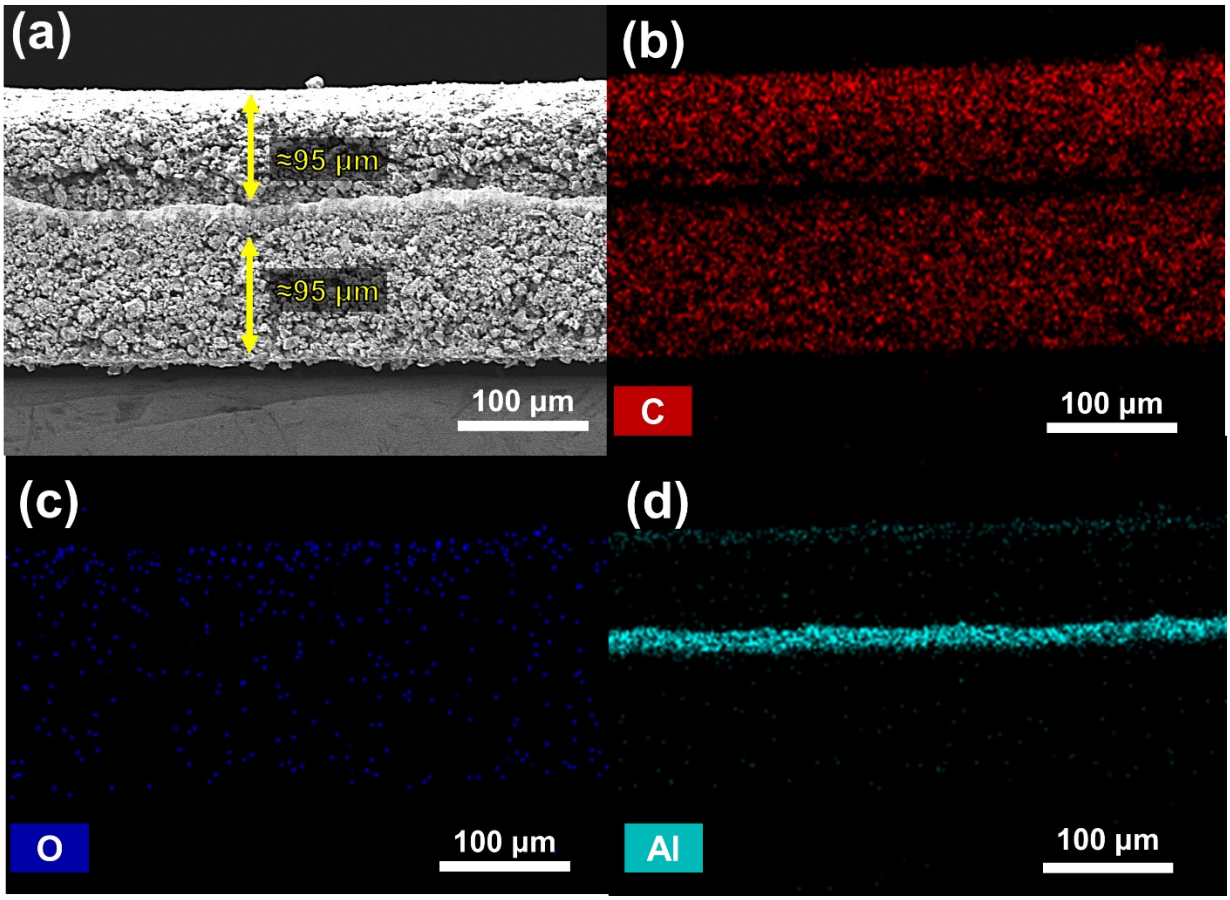

Fig. S8 Physicochemical properties of electrode. (a) Cross-sectional FE-SEM image, (b-d) EDS elemental mapping of C, O and Al, respectively.

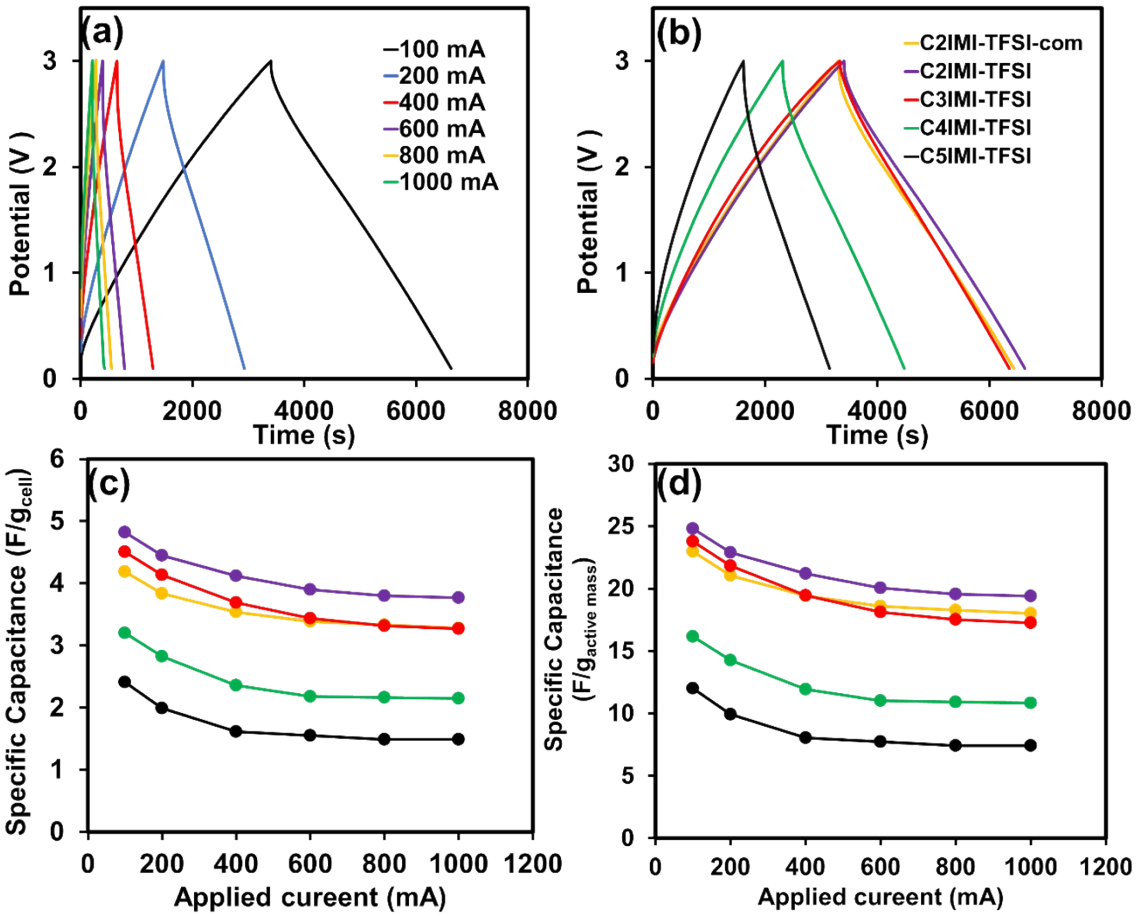

Fig. S9 Electrochemical performance of 18650 supercapacitors. GCD profiles of C2IMI-TFSI at various applied currents (a), GCD plots of all RTILs at 100 mA of applied current (b), gravimetric capacitance in terms of cell mass (c) and active material mass (d). Note that orange, purple, red, green and black represent to C2IMI-TFSI com, C2IMI-TFSI, C3IMI-TFSI, C4IMI-TFSI and C5IMI-TFSI.

Table S1 Performance of ILs on AC electrode from CVs of 3 electrodes set up.

SCs with ILs	Gravimetric capacitance (F/g)							
	5 mV/s	10 mV/s	25 mV/s	50 mV/s	75 mV/s	100 mV/s	250 mV/s	500 mV/s
C2IMI-TFSI	265.8	235.0	172.3	150.4	136.3	126.6	95.0	69.9
C3IMI-TFSI	181.8	167.4	123.7	115.0	102.8	94.2	62.4	39.8
C4IMI-TFSI	162.4	153.1	123.6	106.4	85.3	73.4	40.5	16.3
C5IMI-TFSI	106.4	90.3	78.3	65.1	56.0	48.4	27.8	16.3

Table S2 The impedance data from equivalent circuit of each IL in half-cell set up.

Sample	R_s (Ω)	R_{ct} (Ω)
C2IMI-TFSI	36.8	5.2
C3IMI-TFSI	52.7	9.8
C4IMI-TFSI	66.2	28.2
C5IMI-TFSI	79.9	38.6

Table S3 Specific capacitance of 18650 supercapacitor divided by cell weight.

SCs with ILs	Gravimetric capacitance (F/g)					
	100 mA	200 mA	400 mA	600 mA	800 mA	1000 mA
C2IMI-TFSI	4.82	4.45	4.12	3.90	3.80	3.77
C3IMI-TFSI	4.51	4.34	3.69	3.44	3.32	3.27
C4IMI-TFSI	3.12	2.82	2.36	2.18	2.16	2.15
C5IMI-TFSI	2.41	1.99	1.61	1.55	1.49	1.47

Table S4 Specific capacitance of 18650 supercapacitors divided by active material.

SCs with ILs	Gravimetric capacitance (F/g)					
	100 mA	200 mA	400 mA	600 mA	800 mA	1000 mA
C2IMI-TFSI	24.81	22.90	21.21	20.06	19.57	19.41
C3IMI-TFSI	23.79	21.83	19.46	18.14	17.52	17.26
C4IMI-TFSI	16.16	14.27	11.92	11.02	10.92	10.85
C5IMI-TFSI	12.01	9.91	8.03	7.73	7.42	7.40

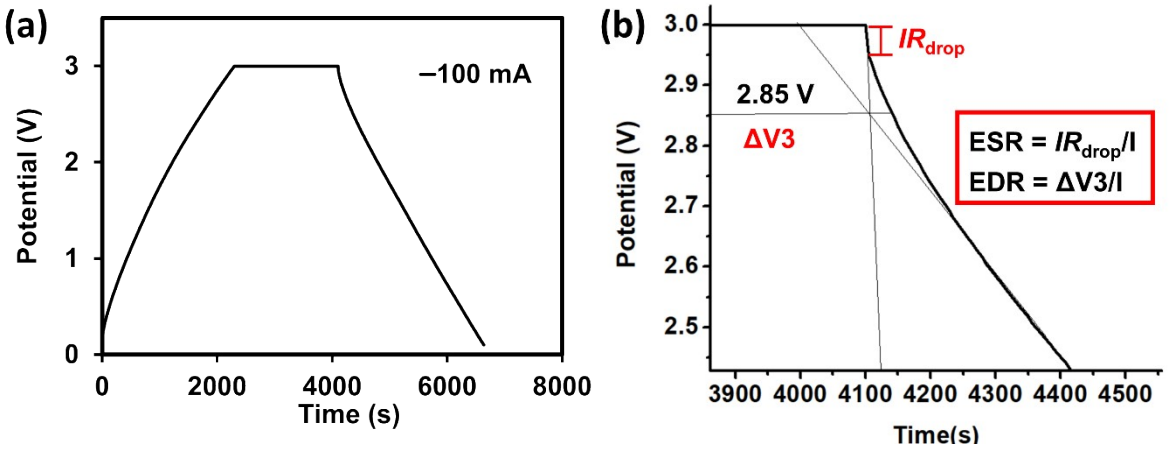

Fig. S10 GCD profile at applied current of 100 mA of 18650-cell with C2IMI-TFSI (a) and method for calculating ESR and EDR (b).

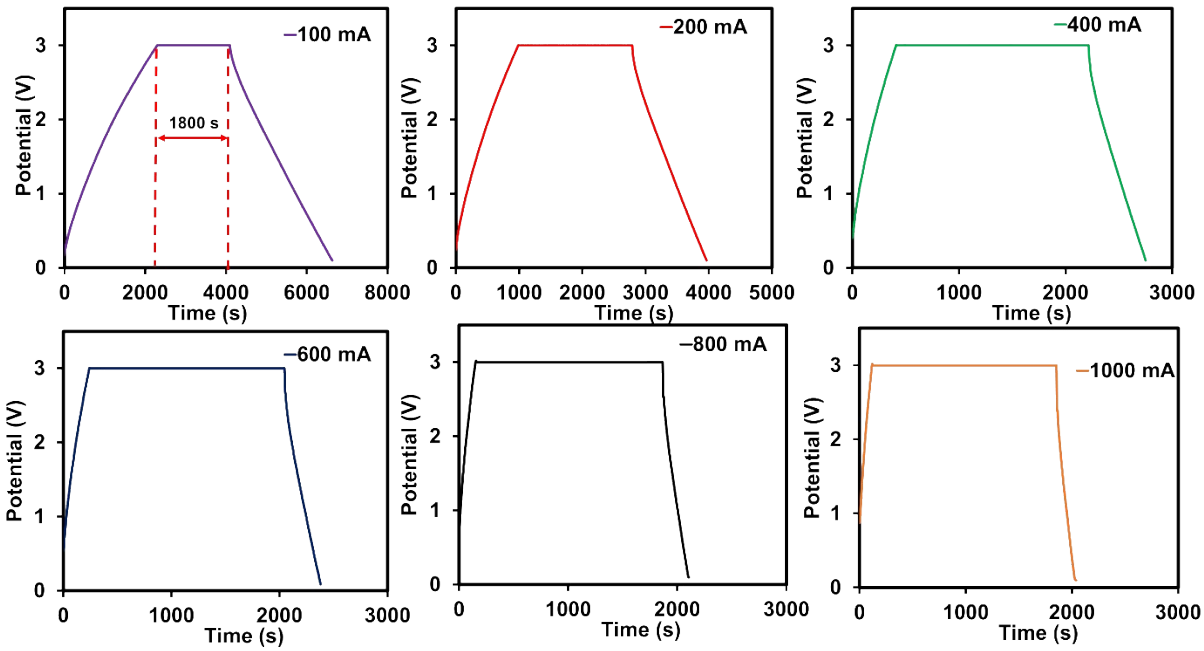

Fig. S11 GCD of 18650-cell with C2IMI-TFSI for calculating ESR and EDR.

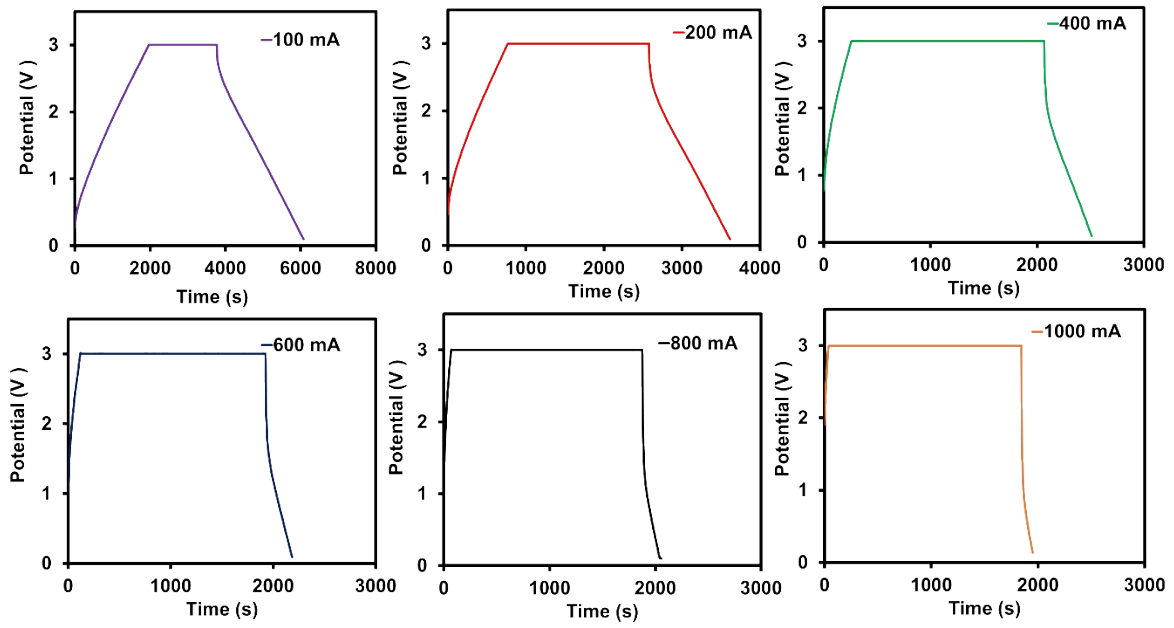

Fig. S12 GCD of 18650-cell with C3IMI-TFSI for calculating ESR and EDR.

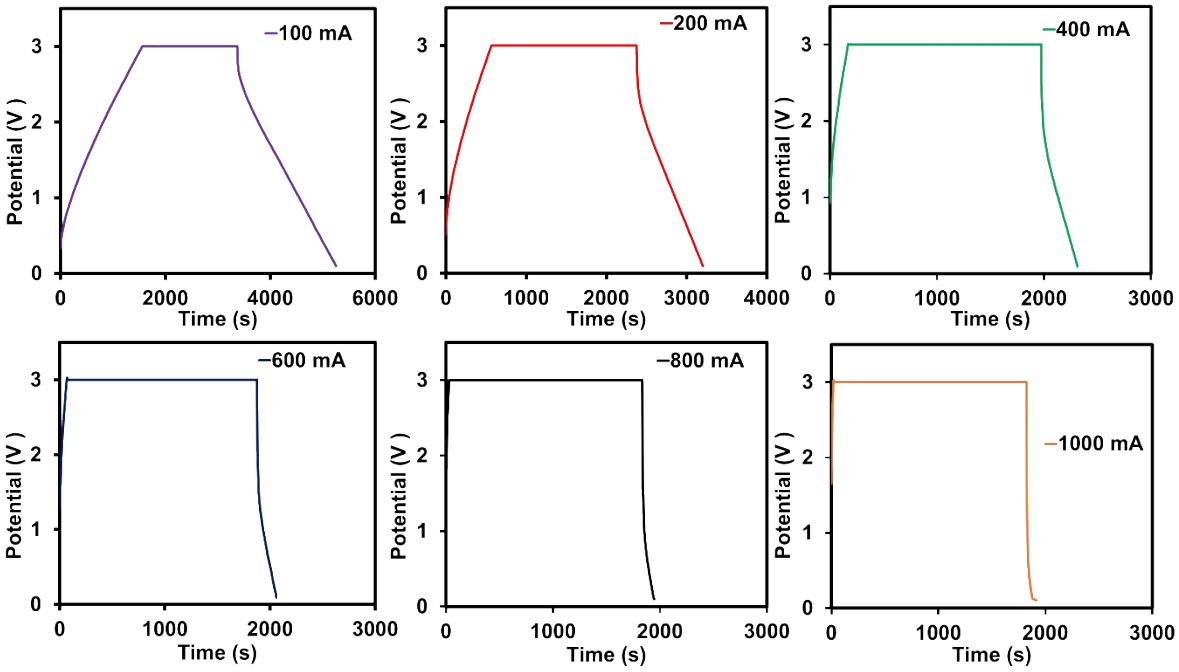

Fig. S13 GCD of 18650-cell with C4IMI-TFSI for calculating ESR and EDR.

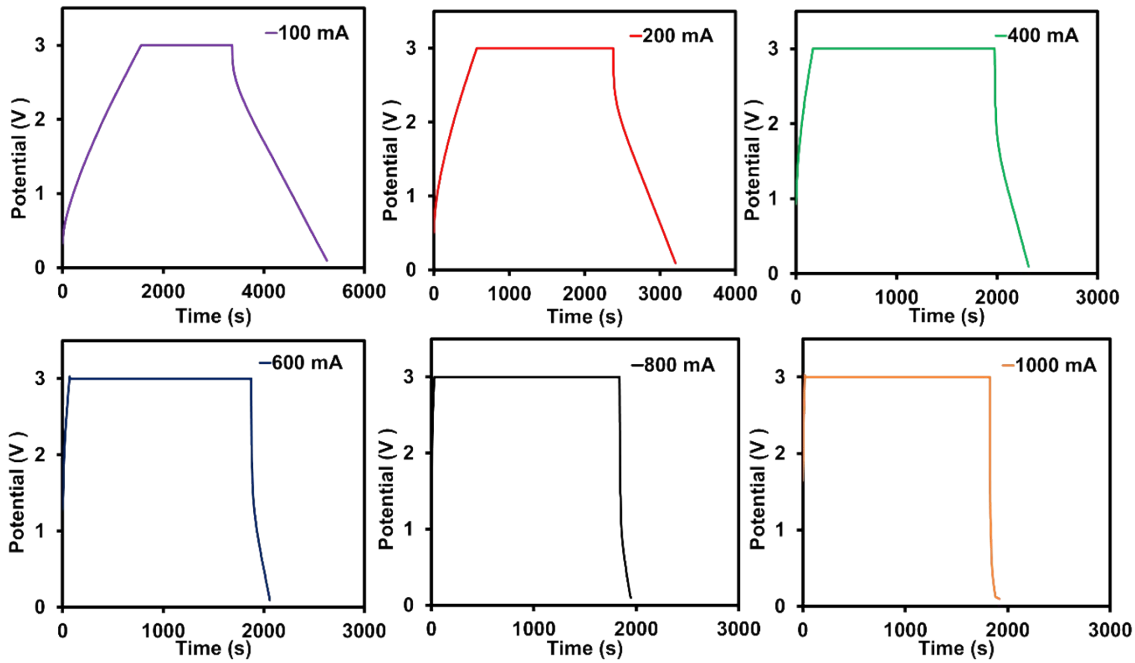

Fig. S14 GCD of 18650-cell with C5IMI-TFSI for calculating ESR and EDR.

Table S5 ESR of 18650-cell with different ILs calculated from GCD.

18650-cell with samples	ESR at applied current					
	100 mA (Ω)	200 mA (Ω)	400 mA (Ω)	600 mA (Ω)	800 mA (Ω)	1000 mA (Ω)
C2IMI-TFSI	0.51	0.49	0.47	0.48	0.49	0.50
C3IMI-TFSI	1.46	1.44	1.43	1.42	1.42	1.42
C4IMI-TFSI	1.78	1.78	1.76	1.76	1.78	1.62
C5IMI-TFSI	1.98	1.98	1.96	1.96	1.98	1.92

Table S6 EDR of 18650-cell with different ILs calculated from GCD.

18650-cell with samples	EDR at applied current					
	100 mA (Ω)	200 mA (Ω)	400 mA (Ω)	600 mA (Ω)	800 mA (Ω)	1000 mA (Ω)
C2IMI-TFSI	1.59	1.50	1.22	0.93	0.90	0.85
C3IMI-TFSI	4.21	3.30	2.73	2.26	2.15	2.02
C4IMI-TFSI	5.25	3.63	3.12	2.81	2.56	2.03
C5IMI-TFSI	5.55	3.93	3.42	2.98	2.66	2.43

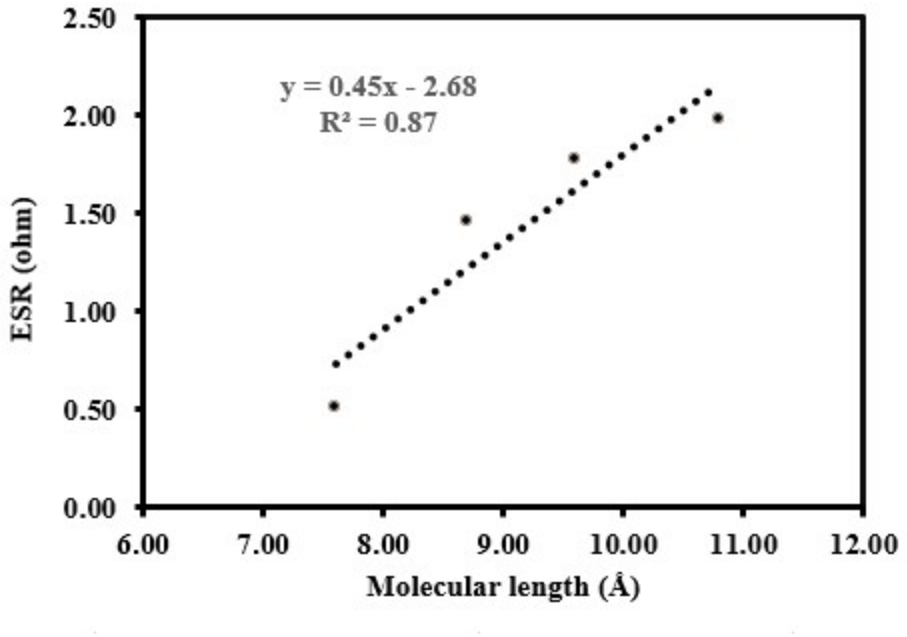

Fig. S15 A linear function relationship of ESR (ohm) determined at 100 mA versus the cationic molecular length at the practical cell level.

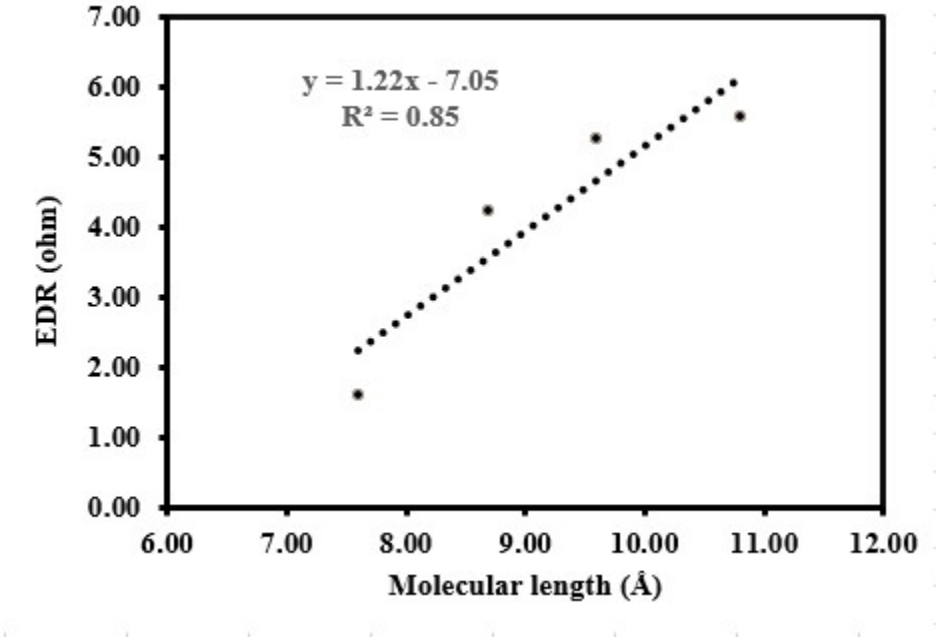

Fig. S16 A linear function relationship of EDR (ohm) determined at 100 mA versus the cationic molecular length at the practical cell level.

Table S7 The impedance data from equivalent circuit of each IL in 18650 cylindrical cells.

Sample	R_s (Ω)	R_{ct} (Ω)
C2IMI-TFSI	0.47	0.12
C3IMI-TFSI	0.51	0.28
C4IMI-TFSI	0.48	0.35
C5IMI-TFSI	0.50	0.46

References

1. K. Pilar, A. Rua, S. N. Suarez, C. Mallia, S. Lai, J. R. P. Jayakody, J. L. Hatcher, J. F. Wishart and S. Greenbaum, *Journal of The Electrochemical Society*, 2017, **164**, H5189-H5196.
2. M. Sawangphruk, M. Suksomboon, K. Kongsupornsak, J. Khuntilo, P. Srimuk, Y. Sanguansak, P. Klunbud, P. Suktha and P. Chiochan, *Journal of Materials Chemistry A*, 2013, **1**, 9630-9636.
3. P. Iamprasertkun, A. Krittayavathananon and M. Sawangphruk, *Carbon*, 2016, **102**, 455-461.
4. A. Krittayavathananon, P. Iamprasertkun and M. Sawangphruk, *Carbon*, 2016, **109**, 314-320.
5. T. Pettong, P. Iamprasertkun, A. Krittayavathananon, P. Sukha, P. Sirisinudomkit, A. Seubsai, M. Chareonpanich, P. Kongkachuichay, J. Limtrakul and M. Sawangphruk, *ACS Applied Materials and Interfaces*, 2016, **8**, 34045-34053.
6. N. Phattharasupakun, J. Wutthiprom, P. Chiochan, P. Suktha, M. Suksomboon, S. Kalasina and M. Sawangphruk, *Chemical Communications*, 2016, **52**, 2585-2588.
7. S. Kalasina, N. Phattharasupakun, T. Maihom, V. Promarak, T. Sudyoadsuk, J. Limtrakul and M. Sawangphruk, *Scientific Reports*, 2018, **8**, 12192.
8. A. Singh and A. Chandra, *Scientific Reports*, 2015, **5**, 15551.
9. V. Ganesh, S. Pitchumani and V. Lakshminarayanan, *Journal of Power Sources*, 2006, **158**, 1523-1532.
10. Q. Wang, B. Qin, X. Zhang, X. Xie, L. e. Jin and Q. Cao, *Journal of Materials Chemistry A*, 2018, **6**, 19653-19663.